Electronic Supplementary Information

Exploring the dual functionality of an ytterbium complex for luminescence thermometry and slow magnetic relaxation

Gabriel Brunet,[a] Riccardo Marin,[a] Melissa-Jane Monk,[b] Ute Resch-Genger,[b] Diogo A. Gálico,[c] Fernando A. Sigoli,[c] Elizaveta A. Suturina,[d] Eva Hemmer,[a] and Muralee Murugesu,[a]*

[a] Department of Chemistry and Biomolecular Sciences, University of Ottawa, 10 Marie Curie, Ottawa, ON, K1N 6N5, Canada. Email: m.murugesu@uottawa.ca

[b] Federal Institute for Materials Research and Testing (BAM), Division Biophotonics, Richard-Willstaetter-Strasse 11, 12489 Berlin, Germany.

[c] Institute of Chemistry – University of Campinas – UNICAMP, P.O. Box 6154, Campinas, Sao Paulo 13083-970, Brazil School of Chemistry.

[d] University of Bath, Claverton Down, Bath, BA2 7AY, UK.

Table of contents

Crystallographic data

Table S1: Crystallographic data for $[Yb_2(valdien)_2(NO_3)_2]$:

Compound	**$[Yb_2(valdien)_2(NO_3)_2]$**
Empirical Formula	$Yb_2C_{40}H_{46}N_8O_{14}$
Crystal system	Triclinic
Space group	*P*–1
a (Å)	10.4586(16)
b (Å)	10.5142(16)
c (Å)	11.4718(17)
α (°)	66.542(3)
β (°)	65.408(3)
γ (°)	79.755(3)
V (Å^3)	1052.1(3)
Z	1
ρ_{calc} (g cm^{-3})	1.908
λ (Å)	0.71073
T (K)	200(2)
μ (mm^{-1})	4.496
F (000)	594
Reflections Collected	26830
Independent Reflections	5220
Reflections with I > 2σ(*I*)	5064
Goodness of fit on F^2	1.068
R_1, wR_2 ($I > 2\sigma(I)$)[a]	0.0115, 0.0297
R_1, wR_2 (all data)	0.0121, 0.0299

[a] $R = R_1 = \sum||F_o| - |F_c||/\sum|F_o|$; $wR_2 = \{\sum[w(F_o^2 - F_c^2)^2]/\sum[w(F_o^2)^2]\}^{1/2}$; $w = 1/[\sigma^2(F_o^2)+(ap)^2 + bp]$, where $p = [\max(F_o^2, 0) + 2F_c^2]/3$; and $Rw = [w(|F_o| - |F_c|)^2 / w|F_o|^2]^{1/2}$, where $w = 1 / \sigma^2(|F_o|)$.

Table S2: Selected bond distances and angles

Select bond distances (Å)			
Yb1-N1	2.4713(14)	Yb1-O3	2.2833(11)
Yb1-N2	2.4962(14)	Yb1-O3a	2.2976(11)
Yb1-N3	2.4885(14)	Yb1-O5	2.4771(13)
Yb1-O2	2.1503(12)	Yb1-O6	2.3843(12)
Select angles (°)			
Yb1-O3-Yb1a	108.37(4)		

Magnetic data

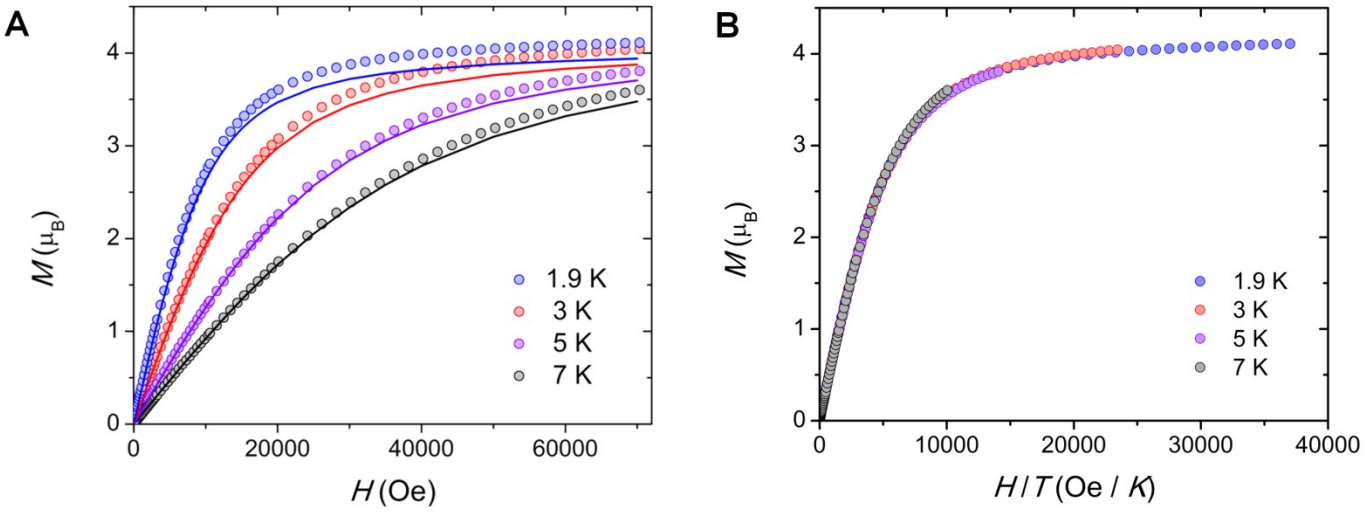

Fig. S1: Experimental (spheres) and calculated (solid lines) field dependence of the magnetization (A) and *M vs*. *H*/*T* plot (B) at the indicated temperatures and up to 7 T.

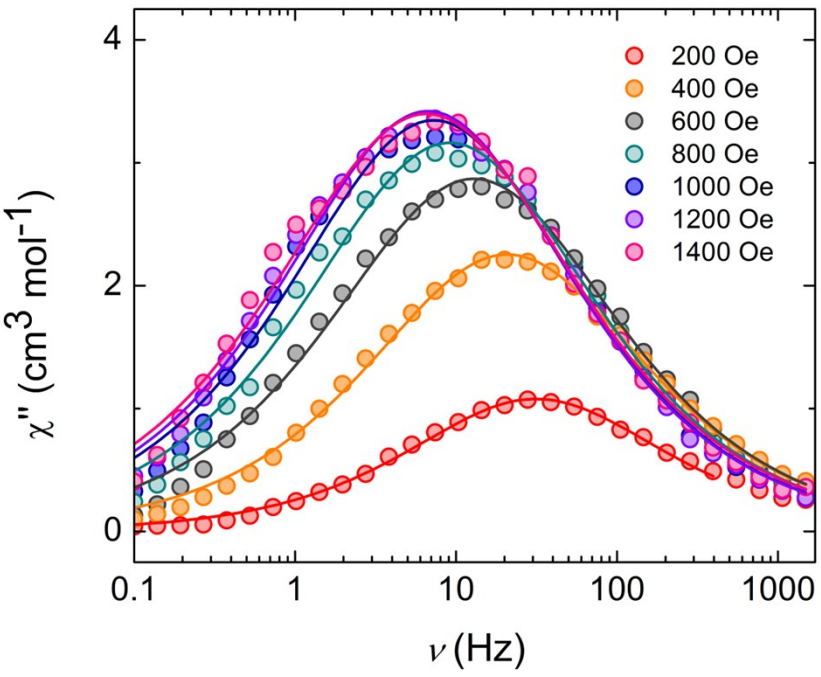

Fig. S2: Frequency dependence of the out-of-phase magnetic susceptibility collected at 1.9 K and at varying fields. The solid lines correspond to the best fit using a generalized Debye model.

Table S3: Values of the relaxation time (τ), α, χ_S and χ_T at 1.9 K under varying dc fields.

***H* (Oe)**	**τ (s)**	**α**	**χ_S**	**χ_T**
200	0.0050(7)	0.299(9)	6.718(0)	10.235(0)
400	0.0076(5)	0.337(7)	6.186(9)	14.055(7)
600	0.012(3)	0.351(7)	5.017(8)	15.299(4)
800	0.017(4)	0.353(3)	4.012(9)	16.377(7)
1000	0.021(8)	0.353(6)	3.723(6)	14.753(2)
1200	0.023(7)	0.356(8)	2.867(9)	15.239(4)
1400	0.024(2)	0.374(3)	2.557(0)	15.255(0)

Table S4: Values of the relaxation time (τ), α, χ_S and χ_T under a 1000 Oe dc field at varying temperatures. Red numbers indicate when values were restrained to remain physically reasonable (*i.e.* $\chi_S \geq 0$).

***T* (K)**	**τ (s)**	**α**	**χ_S**	**χ_T**
1.8	0.022(9)	0.358(5)	0.125(9)	5.612(8)
1.9	0.029(5)	0.347(0)	0.0895(4)	5.244(0)
2.0	0.019(3)	0.345(5)	0.0714(4)	5.036(5)
2.5	0.011(9)	0.316(4)	0.0653(2)	3.912(3)
3.0	0.0073(3)	0.286(4)	0.0533(5)	3.285(2)
3.5	0.0041(9)	0.227(0)	0.00161(1)	2.705(3)
4.0	0.0021(6)	0.165(9)	0.00396(2)	2.343(4)
4.5	0.0010(8)	0.103(2)	$7.48(6) \times 10^{-4}$	2.015(3)
5.0	$5.7(0) \times 10^{-4}$	0.078(6)	$5.45(9) \times 10^{-4}$	1.809(6)
5.5	$3.2(2) \times 10^{-4}$	0.057(5)	$1.45(9) \times 10^{-4}$	1.632(3)
6	$1.9(8) \times 10^{-4}$	0.033(9)	$1.32(4) \times 10^{-4}$	1.481(8)
6.5	$1.1(4) \times 10^{-4}$	0.034(9)	$1.13(3) \times 10^{-4}$	1.412(1)
7.0	$7.4(8) \times 10^{-5}$	0.018(9)	0	1.321(4)
8.0	$2.7(5) \times 10^{-5}$	0.009(8)	0	1.294(1)

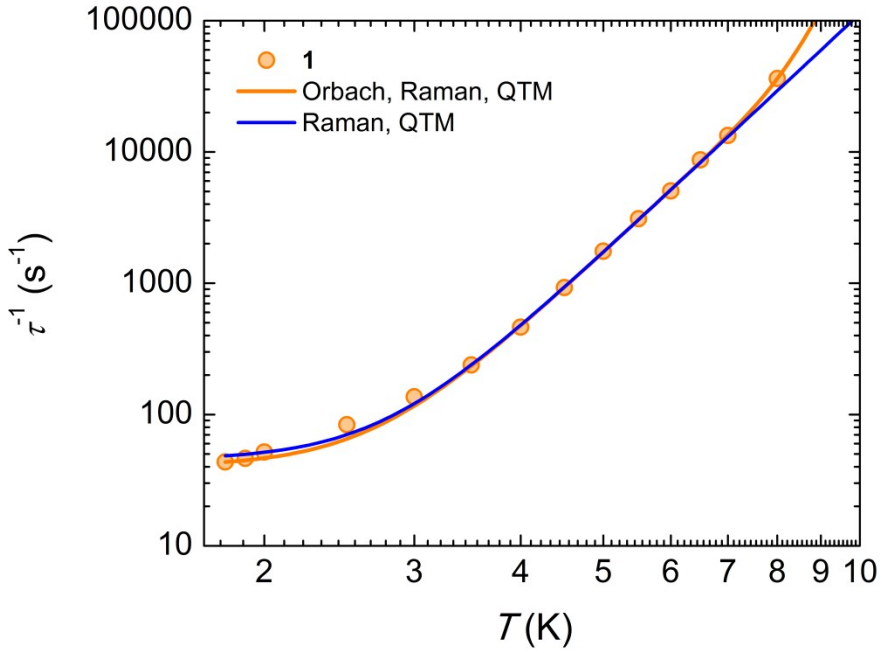

Fig. S3: Temperature dependence of the relaxation times plotted as τ^{-1} *vs.* T and under an applied field of 1000 Oe. Here we compare the best-fits obtained from Orbach/Raman/QTM (orange line) and Raman/QTM (blue line).

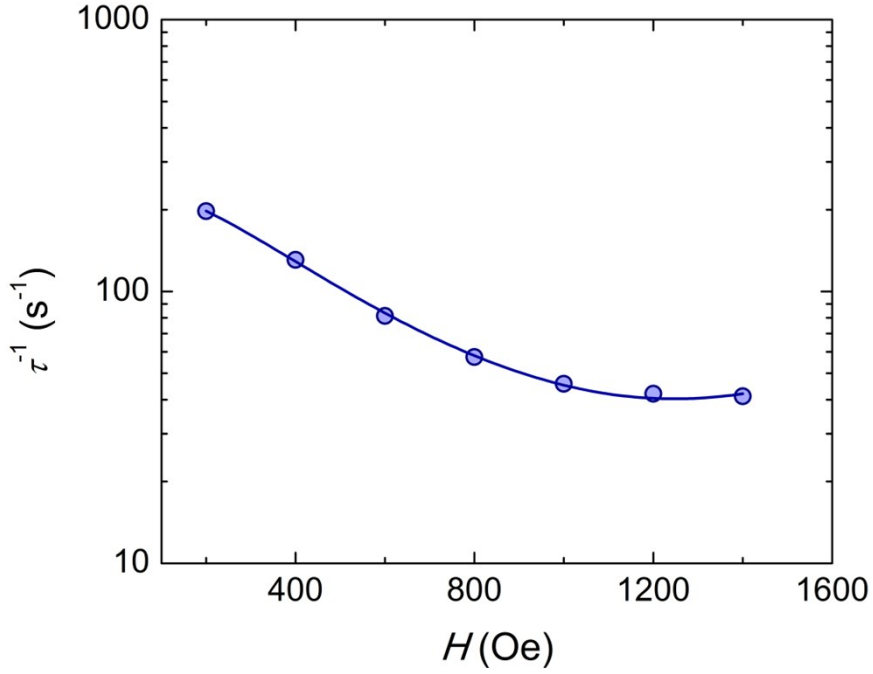

Fig. S4: Field dependence of the relaxation time plotted as τ^{-1} *vs. H* and measured at 1.9 K. The solid line represents the best fit using the model described in the main text.

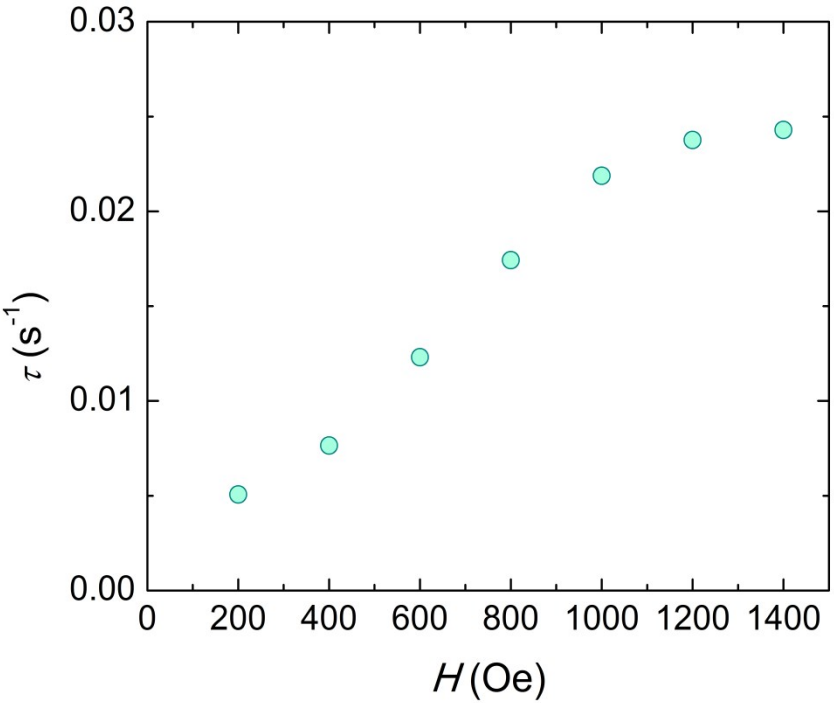

Fig. S5: Field dependence of the relaxation time plotted as τ *vs. H* and measured at 1.9 K.

Lifetime measurement under direct Yb^{III} excitation

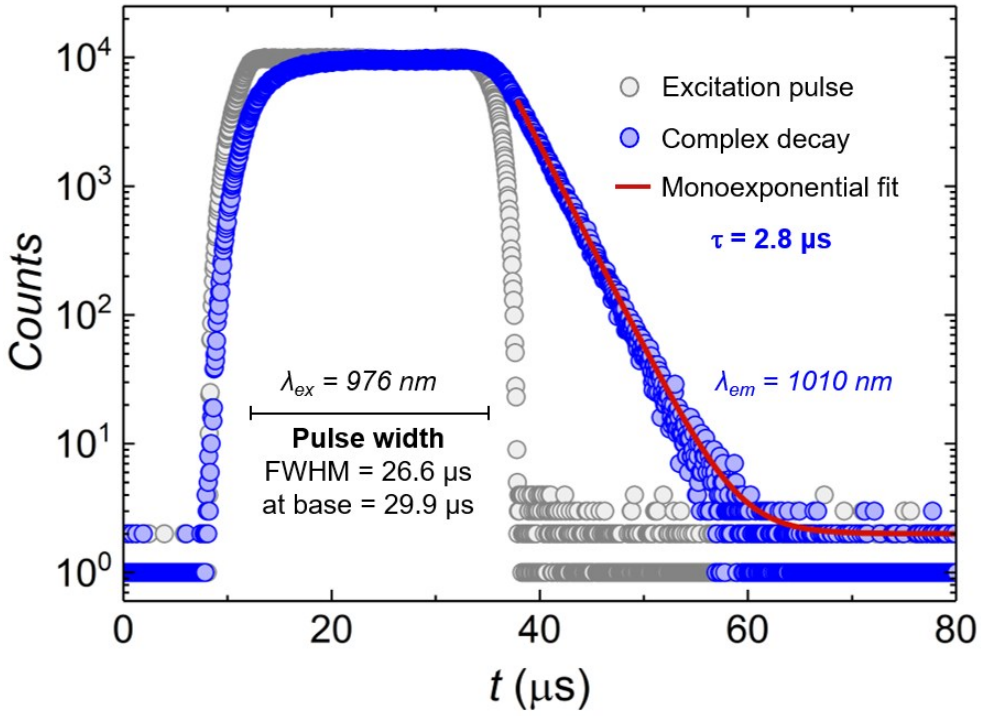

Fig. S6: Photoluminescence decay kinetics recorded under 976 nm excitation and monitoring the Yb^{III} emission at 1010 nm. At this excitation wavelength Yb^{III} is directly excited.

Photoluminescence quantum yield measurement

$$PLQY = N_{em} / N_{abs} \quad \text{(eq. S1)}$$

The photoluminescence quantum yield (PLQY) of the sample was calculated from the number of emitted photons (N_{em}) and the number of absorbed photons (N_{abs}) at the excitation wavelength using equation S1 as previously described.[1] As non-emissive blank, measured under identical conditions used for the emissive sample, either a cell filled with $BaSO_4$ powder or an empty cell were used. The absorbed photon flux and the emitted photon flux, required for determining N_{em} and N_{abs}, were obtained by separating the measured spectra of the sample and the blank into an excitation and an emission region. The absorbed photon flux results from the integrated difference of the spectrally corrected signals of the blank and the sample in the spectral range of the excitation, here 362-388 nm, with the blank signal providing the incident photon flux that is weakened by sample absorption. This yields N_{abs}. The emitted photon flux, hence N_{em}, was obtained from the integrated difference of the spectrally corrected sample and blank signals in the spectral region of the Yb^{III} emission, here 900-1060 nm.

Due to the lack of a blank with scattering properties and a reflectivity closely matching that of the sample, two different blanks of varying scattering features and reflectivity were utilized. Scattering $BaSO_4$ powder filled into the measurement cell was chosen as a blank with a high reflectivity and an empty cell was used representatively for a non-scattering blank of low reflectivity. This procedure provides a range of PLQY values for the SMM, thereby accounting for contributions from the non-optimum blanks.

The PLQY values obtained for the Yb^{III} emission of the SMM complex with different measurement procedures, *i.e.* using different blanks (**a** – cuvette filled with $BaSO_4$, **b** – empty cuvette) and integrating ranges, are summarized in Table S5. For each blank, a mean value and relative standard deviation are provided; the number of measurements used for the calculation of the relative standard deviations are also included. As the measurements using the empty cuvette as blank yield a higher uncertainty, the PLQY of the Yb^{III} emission of SMM given in the manuscript was calculated as a mean of the values obtained from the two independent sets of measurements **a** and **b.** This gives a PLQY of 0.43 % when the emission signal is integrated over the range 900-1060 nm. Table S5 highlights also the dependence of the calculated PLQY of the Yb^{III} emission on the chosen range of integration. This influence is evident from Figure S7, displaying the Yb^{III} emission, stretching from roughly 900 nm to 1150 nm, and the different integration ranges used for the calculations of the PLQY values reported in Table S5. For example, the use of the wavelength range 965-990 nm, centred in correspondence of the sharp band at 978 nm, yields a PLQY value of only 0.11%. This underlines the need for providing the integration range used to assess PLQY data.

Table S5: Summary of the results obtained from the PLQY calculation using different integration ranges.

Measurement	*PLQY[1] (%)*	*std. dev.*	*rel. std. dev.*	*blank*	*repetitions*	*PLQY[2] (%)*	*PLQY[3] (%)*	*PLQY[4] (%)*
a	0.50	0.06	14%	$BaSO_4$	3	0.05	0.12	0.33
b	0.37	0.08	20%	empty cell	12	0.04	0.11	0.22
Mean [**a**;**b**]	0.43	0.07	14%					

[1] integration range 900-1060 nm
[2] integration range 900-965 nm
[3] integration range 965-990 nm
[4] integration range 990-1060 nm

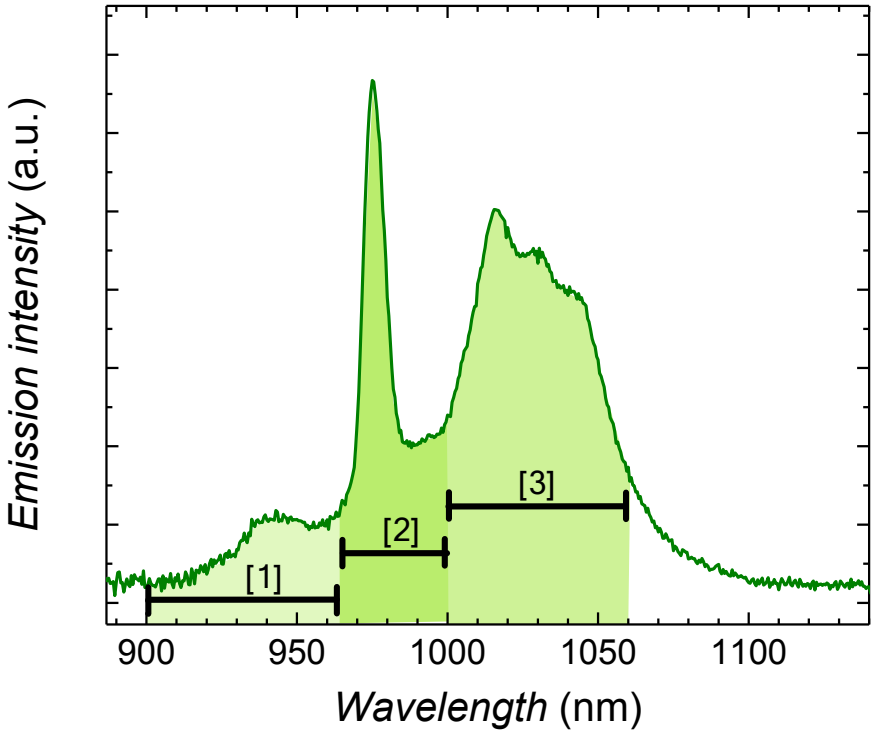

Fig. S7. Emission spectrum of the SMM under study presenting the assigned integration ranges [1], [2], [3] used for the alternative calculation of the PLQY values reported in Table S5

The integration range used for the Yb^{III} emission can be also affected by the detection system used as the wavelength region of about 950 nm to 1100 nm is particularly challenging. This is highlighted in Figure S8 comparing the Yb^{III} emission spectra obtained with two instruments using different types of detectors, here a silicon CCD used as detection system for the integrating sphere setup and

different PMTs employed as detectors for the spectrofluorometer. Due to the limited spectral sensitivity of the silicon CCD at wavelengths above 1000 nm, the Yb^{III} emission band could not be fully resolved with the integrating sphere setup and was cut off at 1060 nm. This leads to an underestimation of the absolutely measured PLQY by approximately 10 %. Considering this underestimation, the PLQY could reach up to 0.47 % for the integrating range from 900 to 1150 nm.

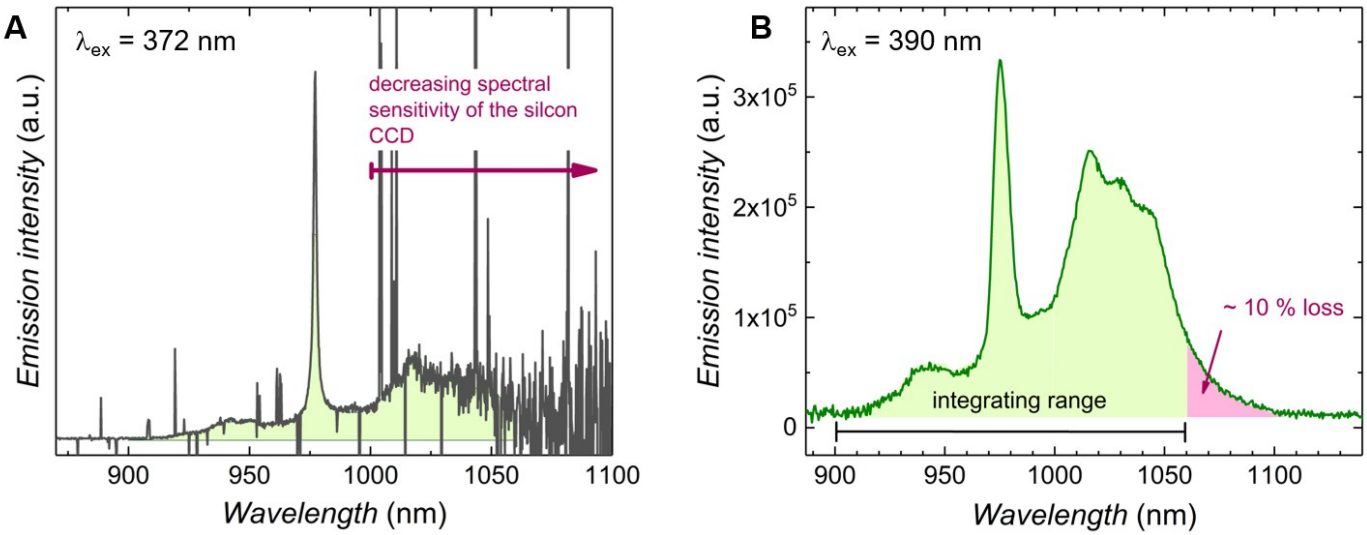

Fig. S8. Ligand-sensitized emission spectrum of the proposed SMM obtained in the integrating sphere setup (A) and the spectrofluorometer FSP920 by Edinburgh Instruments equipped with three different detectors covering the wavelength range from about 300 to 1700 nm (B). For the measurements shown here, a NIR_R5509P detector was used.

Discussion over photoluminescence quantum yield measurements

The PLQY of the system under study was calculated to be in the range 0.4-0.5% This value is in line with others reported in the literature for Yb^{III} complexes (values of selected systems are presented in Table S6). However, it is important to consider that the system under study represents a particularly challenging one in terms of absolute PLQY determination because of its relatively small PLQY, the wavelength region of its emission (which is not sensitively covered by many common detection systems, particularly not by silicon and InGaAs CCDs typically used as detectors for integrating sphere spectroscopy), and the lack of a non-emissive blank with a truly matching reflectivity (as often encountered for crystalline samples).

As briefly mentioned in the main text, many variables contribute to complicate PLQY measurements. This in turn hampers a comparison of PLQY values obtained for different systems measured under different experimental conditions and with different experimental setups. Major hurdles are:

1- The spectral correction of the emission signal accounting for the instrument´s wavelength-dependent spectral responsivity[2] is challenging in the spectral region of Yb^{III} emission. This is particularly true above 1000 nm where the sensitivity of frequently used silicon CCDs steeply decreases (see Figure S8) and the sensitivity of InGaAs CCDs is often not yet sufficient to detect very weak signals.
2- Reabsorption of the Yb^{III} emission by Yb^{III} is of great importance for measurements of solid samples with an integrating sphere with its enhanced optical pathlengths.[3]
3- The choice of a suitable blank for measurements of crystals and powders represents a major hurdle to the measurements.[4] Only a wise choice of the blank (with a reflectivity closely matching that of the sample) allows for the precise determination of the number of photons incident on the sample during the absolute measurement of PLQY.
4- The wavelength range used for the integration of the emission has a major impact on the obtained PLQY value as highlighted in the previous section, in Table S5 and in Figures S7 and S8.

All this given, the PLQY values of our Yb^{III} SMM fall within the range of PLQY values observed by other groups for Yb^{III} complexes in solution, in solid matrices (*e.g.* polymers), and in the crystalline or powdered state. The photoluminescence properties of selected Yb^{III} complexes in different matrices and aggregation states are exemplarily given in Table S6. For these results reported by other groups, similar shortcomings of the measurement, therefore similarly high uncertainties in the order of up to 30%, should be taken into account (these uncertainties are those derived from uncertainty budgets, *i.e.* summing up uncertainties from all possible sources of uncertainty including those resulting from instrument calibration and

the actual measurements; we are not simply referring to the relative standard deviations of the fluorescence measurements).[5,6] Moreover, frequently, neither the instrument calibration nor other parameters affecting resulting PLQY values - like the wavelength range used for integration of the Yb^{III} emission band - are provided. This point is of great relevance for Yb^{III}, the emission of which extends over the broad and particularly challenging wavelength region from 900 to 1100 nm (see Fig. 4 and 5 in the main text). This surely affects the comparability of PLQY data of Yb^{III} complexes.

Table S6. Comparison of lifetime and PLQY values as well as measurement methods for selected Yb^{III} systems reported in the literature.

Ligands	***Matrix***	***Excitation λ* (nm)**	***Lifetime* (μs)**	***PLQY* (%)**	***PLQY measurement method***	***Integration range* (nm)**	***Reference***
Valdien	Crystal	372	2.5-2.8	0.43	Integrating sphere (***absolute method***)	900-1060	This work
(Z)-4-(hydroxyimino)-3-methyl-1-phenyl-1H-pyrazol-5(4H)-one + 1.10-phenantroline	CCl_4, PMMA	355	54, 12	2.3, 1	From lifetime measurements	N/A	7
N,N′-bis(salicylidene)-1,2-phenylenediamine	CH_3CN	412	8-12	0.4-0.6	From lifetime measurements	N/A	8
$[LnGa_4(shi)_4(CH_5CO_2)_4(C_5H_5N)(CH_3OH)]$	Crystal, CD_3OD, CH_3OH	320-350	55.7, 36.6, 2.06	5.88, 4.29, 0.26	Integrating sphere (***absolute method***)	N/A	9
TTF-fused dipyrido[3,2-a:2′,3′-c]-Phenazine + 1,1,1,5,5,5-hexafluoroacetylacetonate + 2-thenoyltrifluoroacetonate	CH_2Cl_2	550	9-10	1	From lifetime measurements	N/A	10
$[(\eta_5\text{-}C_5H_5)Co\text{-}\{(D_3CO)_2P = O\}_3]$-Yb(III)-7,8,12,13,17,18-hexafluoro-5,10,15,20-tetrakis(pentafluorophenyl)porpholactol	CH_2Cl_2	406	20, 40	2.4, 4.5	Comparative method using reference 5,10,15,20-tetraphenylporphyrin-Yb(III)-[(cyclopentadienyl)tris(di(ethyl)-phosphito)cobaltate] in CH_2Cl_2 (PLQY = 0.024%)	880-1150	11
$[Yb(5,7ClQ)_2(H5,7ClQ)_2Cl$	DMSO	543	690	1.2	From lifetime measurements	N/A	12
Porphyrin-based	Toluene, DMSO, H_2O	330, 430	17.5-20.2	1.0-3.5	Integrating sphere (***absolute method***) and using reference $Yb(TTA)_3H_2O$ in toluene, $Yb(TTA)_3$phen in toluene, $Yb(Tpp)_3Tp$ in CH_2Cl_2	N/A	13
thiacalix[4]- arene-p-tetrasulfonate	Water	312-318	0.37-4.35	0.02-0.33	Comparative method using reference Yb-calcein	N/A	14
1,10 -(4,40 -(2,2-bis((4- (4,4,4-trifluoro-3-oxobutanoyl)phenoxy)methyl) propane-1,3-diyl)bis(oxy)bis(4,1-phenylene))bis(4,4,4-trifluorobutane-1,3-dione)	Crystal, DMF	315-365	12.1, 12.3	2.6, 1.8	Comparative method using reference solid $Yb(TTA)_3$phen in an integrating sphere	N/A	15
phenylenevinylenedicarboxylate-3	Water	450	7.01	0.01	Comparative method using reference solid $Yb(TTA)_3$phen in DMSO (PLQY = 0.19%)	N/A	16
2,3,7,8,12,13,17,18-octafluoro-5,10,15,20-tetrakis(pentafluorophenyl) porphyrin	CH_2Cl_2, CD_2Cl_2	414	29-714	2.4-69	Comparative method using reference $Yb(TPP)(L_{OEt})$ in CH_2Cl_2 (PLQY = 2.4%) and integrating sphere (***absolute method***)	N/A	17

Spectral features of the {Yb_2} emission

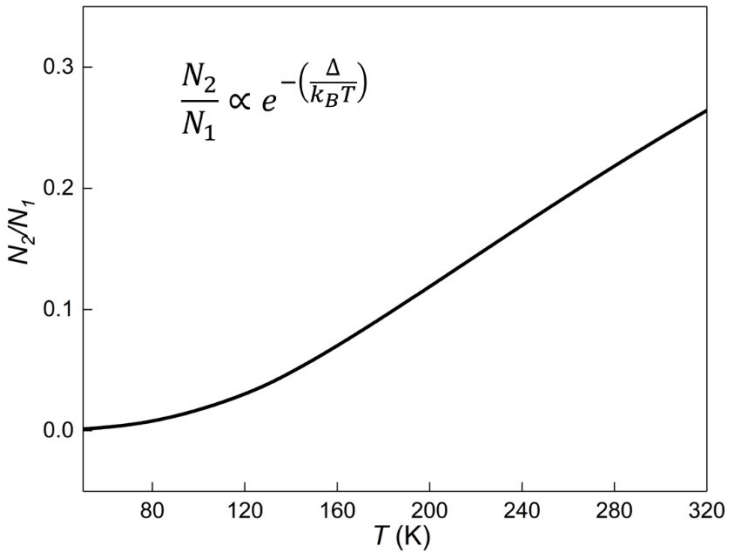

Fig. S9: Relative population of the first two Yb^{III} $^2F_{5/2}$ *Mj* levels as obtained from the Boltzmann distribution. N_2 and N_1 are the electron population in the higher- and lower-energy level, respectively, Δ is the energy difference between the two considered levels and k_B is the Boltzmann constant.

The emission spectrum of {Yb_2} is characterized by broad features the unambiguous identification of which is challenging due to the nature of the investigated compound. For instance, the feature centered around 940 nm presumably follows from a combination of electron population partition between Stark sublevels and vibronic contributions. The energy difference between the first two Yb^{III} $^2F_{5/2}$ *Mj* levels (296 cm^{-1}, as obtained from *ab initio* calculations) is comparable to the energy separation between the 0'-0 line and the examined feature, and the Boltzmann distribution shows that a thermally-activated population of the first excited $^2F_{5/2}$ *Mj* level occurs predominantly in the tested temperature range. This could partially explain the increased intensity of the signal around 940 nm. Additionally, Yb^{III} is prone to marked electron-phonon coupling,[19] in particular when the nature of the chemical bonds is covalent rather than ionic.[20] This fosters the appearance of vibronic sidebands that can heavily contribute to determine the profile of the emission spectrum. In this context, the dinuclear nature of the {Yb_2} complex makes it even more troublesome to univocally assign specific features of the spectrum, due to possible intramolecular Yb^{III}-Yb^{III} interactions.

References

1. M. Kaiser, C, Würth, M. Kraft, I. Hyppanen, T. Soukka and U. Resch-Genger, *Nanoscale* 2017**, 9**, 10051.
2. U. Resch-Genger and P. C. DeRose, *Pure Appl Chem* 2012**, 84**, 1815.
3. S. Hatami, C. Würth, M. Kaiser, S. Leubner, S. Gabriel, L. Bahrig, V. Lesnyak, J. Pauli, N. Gaponik, A. Eychmuller and U. Resch-Genger, *Nanoscale* 2015**, 7**, 133.
4. C. Würth, D. Geissler, T. Behnke, M. Kaiser and U. Resch-Genger, *Anal Bioanal Chem* 2015**, 407**, 59.
5. C. Würth, M. Grabolle, J. Pauli, M. Spieles and U. Resch-Genger, *Anal Chem* 2011**, 83**, 3431.
6. C. Würth, J. Pauli, C. Lochmann, M. Spieles and U. Resch-Genger, *Anal Chem* 2012**, 84**, 1345.
7. A. Sanguineti, A. Monguzzi, G. Vaccaro, F. Meinardi, E. Ronchi, M. Moret, U. Cosentino, G. Moro, R. Simonutti, M. Mauri, R. Tubino and L. Beverina, *Phys Chem Chem Phys* 2012**, 14**, 6452.
8. T. Q. Liu, P. F. Yan, F. Luan, Y. X. Li, J. W. Sun, C. Chen, F. Yang, H. Chen, X. Y. Zou and G. M. Li, *Inorg Chem* 2015**, 54**, 221.
9. C. Y. Chow, S. V. Eliseeva, E. R. Trivedi, T. N. Nguyen, J. W. Kampf, S. Petoud and V. L. Pecoraro, *J Am Chem Soc* 2016**, 138**, 5100.
10. F. Pointillart, J. Jung, R. Berraud-Pache, B. Le Guennic, V. Dorcet, S. Golhen, O. Cador, O. Maury, Y. Guyot, S. Decurtins, S. X. Liu and L. Ouahab, *Inorg Chem* 2015**, 54**, 5384.
11. Y. Ning, Y. W. Liu, Y. S. Meng and J. L. Zhang, *Inorg Chem* 2018**, 57**, 1332.
12. F. Artizzu, F. Quochi, M. Saba, L. Marchiò, D. Espa, A. Serpe, A. Mura, M. L. Mercuri, G. Bongiovanni and P. Deplano, *ChemPlusChem* 2012**, 77**, 240.
13. T. Zhang, X. Zhu, C. C. Cheng, W. M. Kwok, H. L. Tam, J. Hao, D. W. Kwong, W. K. Wong and K. L. Wong, *J Am Chem Soc* 2011, **133**, 20120.
14. N. Iki, S. Hiro-oka, T. Tanaka, C. Kabuto andH. Hoshino, *Inorg Chem* 2012, **51**, 1648.
15. S. Biju, Y. K. Eom, J-C. G. Bünzli and H. K. Kim, *J Mater Chem C* 2013, **1**, 6935.
16. A. Foucault-Collet, K. A. Gogick, K. A. White, S. Villette, A. Pallier, G. Collet, C. Kieda, T. Li, S. J. Geib, N. L. Rosi and S. Petoud, *Proc Natl Acad Sci USA* 2013**, 110**, 17199.
17. J. Y. Hu, Y. Ning, Y. S. Meng, J. Zhang, Z. Y. Wu, S. Gao and J. L. Zhang, *Chem Sci* 2017, **8**, 2702.
18. L. Li, Y. Zhu, X. Zhou, C. D. S. Brites, D. Ananias, Z. Lin, F. A. A. Paz, J. Rocha, W. Huang and L. D. Carlos, *Adv Funct Mater* 2016**, 26**, 8677.
19. A. Ellens, H. Andres, M. L. H. ter Heerst, R. T. Wegh, A. Meijerink and G. Blasse, *J Lumin* 1996, **66-67**, 240.
20. A. Meijerink, G. Blasse, J. Sytsma, C. de Mello Donega and A. Ellens, *Acta Phys Polon A* 1996, **90**, 109.